Astronomy & Astrophysics manuscript no. output
March 26, 2025

Milky Way, Andromeda and seven dwarfs

Danila Makarov[1], Dmitry Makarov[1,⋆], Lidia Makarova[1], and Noam Libeskind[2]

[1] Special Astrophysical Observatory, Russian Academy of Sciences, Nizhnii Arkhyz, 369167 Russia
[2] Leibniz Institut für Astrophysik Potsdam (AIP), An der Sternwarte 16, D-14482, Potsdam, Germany

ABSTRACT

We analyze the velocity field of peripheral members of the Local Group. The Hubble flow at distances from 400 to 1400 kpc, formed by 7 of 11 nearby galaxies, is characterized by an extremely small line-of-sight velocity dispersion of 14 km s^{-1}, which differs significantly from the predictions of cosmological simulations of about 70 km s^{-1}. This fact allows us to determine the total mass of the Local Group as $M_{\rm LG} = (2.46 \pm 0.13) \times 10^{12}\ M_\odot$ using an analytical model of the Hubble flow around a spherical overdensity in the standard flat ΛCDM universe. The practical equality of this mass to the sum of the masses of our Galaxy and the Andromeda Galaxy, as well as the absence of mass growth in the range of distances under consideration, gives grounds to conclude that the entire mass of the Local Group is confined within the virial radii around its two main galaxies. The barycenter, found from the minimal scatter of mass estimates, corresponds to the mass ratio of the Milky Way and the Andromeda Galaxy equal to $M_{\rm MW}/M_{\rm M31} = 0.79 \pm 0.10$. The velocity of our Galaxy to the barycenter turns out to be 61 km s^{-1}. This allows us to determine the apex of the Sun relative to the barycenter of the Local Group to be $(l, b, V) = (+93.9^\circ \pm 0.7^\circ, -2.6^\circ \pm 0.3^\circ, 300 \pm 3$ km s$^{-1})$ in the Galactic coordinates.

Key words. Local Group — Local Group: kinematics and dynamics — dark matter

1. Introduction

Analysis of the kinematics of satellites inside virial zones is the main way to estimate the mass of galactic systems, using various analogues of the virial theorem (Bahcall & Tremaine 1981). In the case of distant systems, we can only measure the line-of-sight velocities and the angular separation between galaxies. Thanks to high-precision distance measurements, we know the three-dimensional distribution of satellites around the Andromeda Galaxy (M 31), which allows us to improve estimates of its mass. Thanks to the Gaia mission (Gaia Collaboration et al. 2018), proper motions have been measured for most of the Milky Way (MW) satellites, unambiguously determining all 6 components of the phase space for each satellite. This information is actively used to clarify the structure of our Galaxy and estimate its total mass.

Dwarf galaxies located outside the virial zones of the MW and M 31 provide an alternative method for estimating the total mass of the Local Group by the deviation of their velocities from the linear Hubble law. Analysis of the peculiar motions of galaxies is a key technique for mapping the distribution of matter on scales from a few to hundreds of megaparsecs. As an example, Tully et al. (2014) discovered the Laniakea supercluster, which includes the Local Supercluster, by the coherent 'flow' of galaxies into this region. The measurement of the zero-velocity sphere radius, also known as the stopping or turning radius, has become the standard method for the total mass estimation of the Local Group (Karachentsev et al. 2009) and other nearby galaxy groups (Kashibadze & Karachentsev 2018). It should be emphasized that inside the stopping radius, falling objects are in a non-linear regime and it is necessary to use more complex models to describe their motion. The exact solution for the Hubble flow (Baushev 2020) for a spherically symmetric distribution of matter gives us a tool to estimate the mass at different distances from the gravitating center.

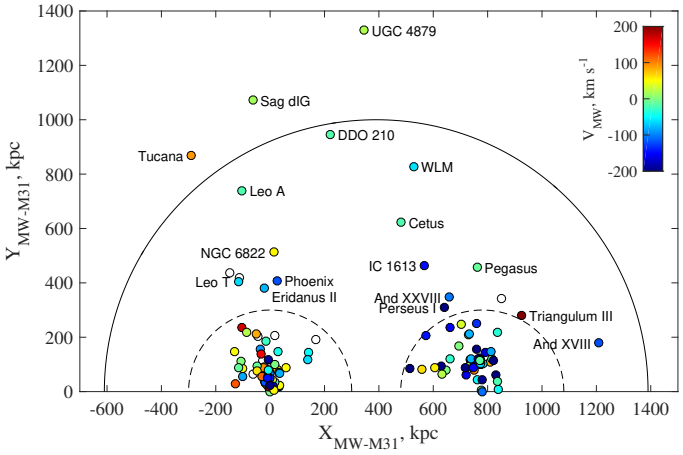

Fig. 1. Distribution of Local Group galaxies in a cylindrical projection, where the X axis is directed from the center of the Milky Way to the center of the Andromeda Galaxy, and the Y axis corresponds to the distance from the X axis. The dashed semicircles with a radius of 300 kpc roughly correspond to the size of the virial zones around the two main galaxies. A solid semicircle with a radius of 1 Mpc shows the approximate boundary of the Local Group. Objects are colored according to their radial velocities relative to the center of our Galaxy. Open dots indicate dwarf galaxies with unknown velocities.

Unfortunately, the structure of the Local Group is more complex. It exhibits the well-known dumbbell-shaped distribution around two giant galaxies of comparable masses, the MW and M 31 (see Fig. 1). All other members of the Local Group are much inferior to them in mass and luminosity. To date, 131 galaxies have been found within 1 Mpc relative to the barycenter of the Local Group. Most of them are concentrated in the virial

⋆ e-mail: dim@sao.ru

zones around the MW and M 31. There are 64 satellites of our Galaxy within 300 kpc and 48 satellites of M 31 within a similar volume. Figure 1 illustrates that dwarf galaxies outside the virial zones are concentrated towards planes passing through the two main galaxies and oriented roughly perpendicular to the MW – M 31 line.

Despite this, we can assume that the differences of the Local Group potential from the spherical symmetry are relatively small at its periphery. Therefore, considering the motions of galaxies relative to the center of mass of the MW and M 31, we can expect that the infall of galaxies into the Local Group is governed by the total mass of the system and directed toward its barycenter.

The aim of the work is to analyze the motion of galaxies outside the virial zones, estimate the total mass of the Local Group based on the shape of the Hubble flow and attempt to measure changes in the mass profile at the periphery of the system.

2. Velocity field model

Despite the fact that proper motions have been measured for a large number of even distant members of the Local Group, these data are of little use for our analysis. For galaxies at distances greater than 300 kpc, errors range from 0.01 to 0.4 mas yr^{-1}, with an average value of 0.14 mas yr^{-1} (Battaglia et al. 2022), which translates into typical velocity errors at such distances of hundreds of km s^{-1}. The proper motion is found to be significant at a level greater than 3 sigma for only two galaxies, NGC 6822 and WLM. But even in these cases, the tangential velocity errors are equal to $\sigma \approx 35$ and 170 km s^{-1} for NGC 6822 and WLM respectively, which is significantly worse than the typical accuracy of line-of-sight velocity measurements of the order of several km s^{-1}. That is why Battaglia et al. (2022) caution the reader that for distant galaxies 'the error in transverse velocity is still too large for scientific applications'. Thus, all further analysis is focused exclusively on the line-of-sight velocities of galaxies.

Figure 2 presents a schematic diagram of the corrections described below. The barycenter of the Local Group is designated as BC. Small letters refer to observed values, and uppercase letters denote values relative to the barycenter. The blue dots indicate real objects: MW, M 31, and a galaxy under consideration. The position of the observer is marked by the Sun symbol. Of course, he is tightly connected to our Galaxy and does not participate in the Hubble flow on its own.

First of all, we take into account the motion of the Sun in the Galaxy, transferring heliocentric velocities, v_h, into the Galactocentric system.

$$v_\mathrm{G} = v_\mathrm{h} + \boldsymbol{V}_\odot \cdot \boldsymbol{n}, \tag{1}$$

where $\boldsymbol{n}$ is an unit direction vector to a galaxy, and $\boldsymbol{V}_\odot$ is the solar velocity vector of $(V_x, V_y, V_z) = (9.5, 250.7, 8.56)$ km s^{-1} in Galactic coordinates with respect to the MW center (Akhmetov et al. 2024). It is based on 18 years of observations of the proper motion of Sgr A* (Reid & Brunthaler 2020) and the distance of $d^\mathrm{MW} = 8249 \pm 9 \pm 45$ pc to the central supermassive black hole (GRAVITY Collaboration et al. 2021).

Next, we assume that the barycenter of the Local Group is mainly determined by its two main galaxies and lies on the line connecting the centers of MW and M 31. Given the MW-to-M 31 mass ratio, x, the position of the center of mass, $\boldsymbol{d}^\mathrm{BC}$, is determined by the following equation.

$$\boldsymbol{d}^\mathrm{BC} = \frac{x}{1+x}\boldsymbol{d}^\mathrm{MW} + \frac{1}{1+x}\boldsymbol{d}^\mathrm{M31}, \tag{2}$$

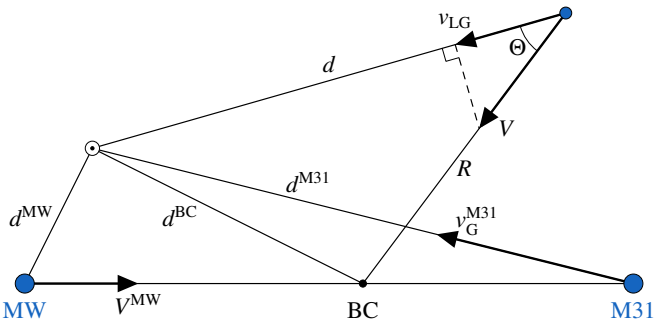

Fig. 2. Scheme for calculating the velocity field in the vicinity of the Local Group. The symbol ⊙ marks the location of the observer. The positions of MW, M 31 and the galaxy under study are shown as blue dots. The barycenter (BC) of the Local Group is marked with a black dot. Corresponding distances and velocity vectors are labeled according to the text.

where $\boldsymbol{d}^\mathrm{MW}$ and $\boldsymbol{d}^\mathrm{M31}$ are the positions of the Milky Way and the Andromeda Galaxy, respectively.

Then, knowing the velocity vector of the Andromeda Galaxy relative to our Galaxy and the mass ratio of these galaxies, we can determine the MW velocity vector relative to the barycenter of the Local Group. The heliocentric velocity of M 31 is known with good accuracy $v_\mathrm{h}^\mathrm{M31} = -301.0 \pm 1.0$ km s^{-1} (Watkins et al. 2013) and, after correction for the motion of the Sun, we determine its Galactocentric velocity equal to $v_\mathrm{G}^\mathrm{M31} = -109 \pm 2$ km s^{-1}. Salomon et al. (2021) note that the M 31 transverse velocity remains poorly determined and conclude that the approach of these two giant galaxies is radial. In agreement with this conclusion, we also assume that the tangential velocity of the Andromeda Galaxy is zero. Thus, the motion of our Galaxy to the barycenter of the Local Group is described by the equation.

$$\boldsymbol{V}^\mathrm{MW} = \frac{v_\mathrm{G}^\mathrm{M31}}{1+x}\boldsymbol{n}^\mathrm{MW-M31}, \tag{3}$$

where the unit vector $\boldsymbol{n}^\mathrm{MW-M31} = (\boldsymbol{d}^\mathrm{M31} - \boldsymbol{d}^\mathrm{MW})/|\boldsymbol{d}^\mathrm{M31} - \boldsymbol{d}^\mathrm{MW}|$ defines the direction from the center of MW to the center of M 31. The appropriate correction to the observed line-of-sight velocity for the velocity of the Galaxy in the Local Group is

$$v_\mathrm{LG} = v_\mathrm{G} + \boldsymbol{V}^\mathrm{MW} \cdot \boldsymbol{n}, \tag{4}$$

where, as before, $\boldsymbol{n}$ is the unit direction to a galaxy,

Then, assuming that the outer members of the Local Group head toward or away from its barycenter, we can determine their velocity by deprojecting their line-of-sight velocities (after all the corrections described above).

$$V = \frac{v_\mathrm{LG}}{\cos\Theta} \tag{5}$$

The distance of a galaxy from the barycenter is determined in the standard way:

$$\boldsymbol{R} = \boldsymbol{d} - \boldsymbol{d}^\mathrm{BC}. \tag{6}$$

The final touch. The analytical solution obtained by Baushev (2020) for the case of the standard flat ΛCDM universe, $\Omega_\Lambda + \Omega_M = 1$, describes the Hubble flow around the mass concentration as a function of the density enclosed within a sphere of a given radius. Consequently, based on the velocity, V, and separation, R, of a galaxy from the barycenter of the Local Group, we can estimate the total mass at the given distance and try to trace the mass distribution in the system. In our work, we use cosmological parameters of the standard ΛCDM model $\Omega_\Lambda = 0.685 \pm 0.007$, $\Omega_M = 0.315 \pm 0.007$, and $H_0 = 67.4 \pm 0.5$ based on the Planck mission data (Lahav & Liddle 2022).

3. Mass estimation from the Hubble flow model

The Hubble flow as it would look from the Local Group centroid, located strictly midway between the MW and M 31 is shown in Fig. 3. There is a noticeable gap between UGC 4879 at 1.35 Mpc and the next 'cloud' of objects beyond 1.6 Mpc, which includes Antlia B, Sextants B, NGC 3109, Antlia, Sextans A and so on. This gives us a natural upper limit for the use of the model, since the analysis of the motion of these more distant galaxies may need to take into account the influence of neighboring giant galaxies, M 81, M 94, Cen A, NGC 253, and IC 342, located at distances of 3–4 Mpc.

To date, there are 20 known peripheral Local Group members at distances closer than 1400 kpc and beyond 300 kpc around the Milky Way and the Andromeda Galaxy. Their list is given in Table 1. It presents the names, J2000.0 coordinates, distance modulii with errors, indicating the method and source of the data, the observed heliocentric velocities with errors, and also the source of the information. The last two columns give the distance from the center of MW and M 31, respectively. High-precision distances for all of these galaxies are known, while the radial velocities for three of them have not yet been measured.

As can be seen in Figure 3, the motion of distant members of the Local Group is fairly regular. With the exception of six galaxies (And XXVIII, Triangulum III, Pegasus, Cetus, NGC 6822 and Tucana), the velocity field outside the virial zones of 300 kpc around the MW and M 31 is reasonably well described by a simple model of the Hubble flow (Baushev 2020) around a point mass.

We have marked objects lying in the 300 to 450 kpc layer from the MW in red (Phoenix, Eridanus II and Leo T), and similarly galaxies around M 31 in magenta (Perseus I, Triangulum III and And XXVIII). In fact, they are located near the virial zones and should be dominated by the nearest giant galaxy, and consequently our simple model of the infall on the center of mass of the Local Group may not work. Moreover, Triangulum III[1] is a satellite of M 33 (Collins et al. 2024). Therefore, it cannot be considered as a free-falling particle. Thus, we do not include these six galaxies in the analysis. Nevertheless, it should be noted that four of them also follow the model quite well.

As a result, our final sample contains 11 galaxies located within 1400 kpc of the Local Group barycenter and at distances greater than 450 kpc from the MW and M 31.

As a first guess, we can estimate the barycenter of the Local Group based on individual masses of MW and M 31. Estimates of the total mass of our Galaxy vary widely from 0.4 to $1.6\times10^{12}\ M_\odot$. Using 33 measurements within 200 kpc compiled by Wang et al. (2020), the average is $(1.07 \pm 0.05) \times 10^{12}\ M_\odot$ with a standard deviation of $0.3\times10^{12}\ M_\odot$. Bobylev & Baykova (2023) obtain a slightly lower value of $(0.88 \pm 0.06) \times 10^{12}\ M_\odot$ with a standard deviation of $0.24\times10^{12}\ M_\odot$ using 20 recent studies. As a rule, the mass measurements of the Andromeda Galaxy give a value 1.5–2 times higher. The average of 7 recent estimates within 300 kpc collected by Bhattacharya (2023) is $(1.61\pm 0.09) \times 10^{12}\ M_\odot$ with the standard deviation of $0.24 \times 10^{12}\ M_\odot$.

Using a modification of the projection mass method (Bahcall & Tremaine 1981), which takes into account the three-dimensional distribution of galaxies in the group and assuming an isotropic distribution of satellite orbits, we estimate of the MW total mass within 240 kpc equal to $M_{\rm MW} = (0.79 \pm 0.23) \times 10^{12}\ M_\odot$ (Makarov et al. 2025). Similarly, we estimate the mass of the M 31 satellite system of $M_{\rm M31} = (1.55 \pm 0.34) \times 10^{12}\ M_\odot$ within 300 kpc.

[1] Triangulum III does not shown in Fig. 3 due to its extremely high peculiar velocity of +333 km s^{-1} with respect to the Local Group centroid.

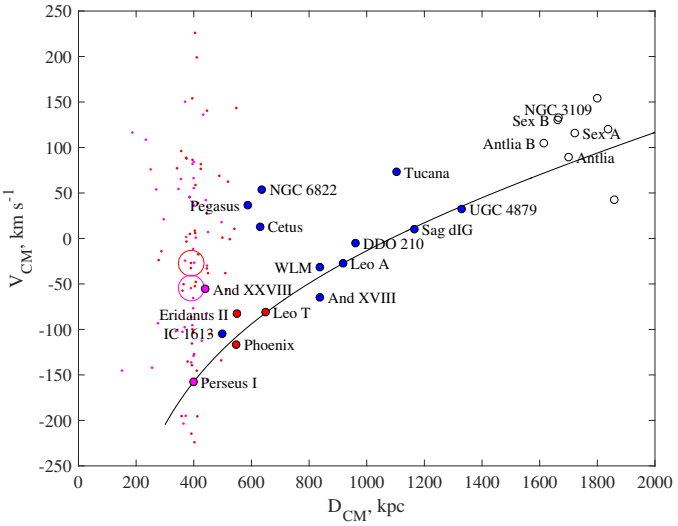

Fig. 3. The Hubble flow with respect to the Local Group center of mass. The big red open circle corresponds to the MW, the small red dots indicate its satellites inside 300 kpc and the filled red circles represent the MW members at distances from 300 to 450 kpc. Likewise, the M 31 and its satellites are shown in magenta. The galaxies selected for the analysis are shown in blue. The solid line corresponds to the Hubble flow model around a point mass of $2.5 \times 10^{12}\ M_\odot$.

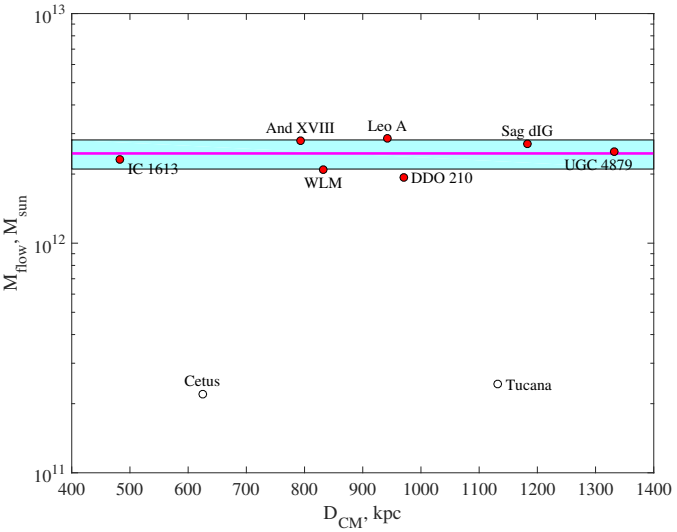

Fig. 4. The total mass of the Local Group from the Hubble flow model versus the distance to the center of mass of the Local Group, which minimizes the spread of the mass estimates.

Taking the mass ratio to be 2.0 from our measurements, we can fix the position of the center of mass of the Local Group and apply the Hubble flow model. Seven of the eleven galaxies give consistent estimates of the total mass of the Local Group with a mean of $M_{\rm LG} = (2.40 \pm 0.22) \times 10^{12}\ M_\odot$ and a surprisingly small spread of $\sigma_M = 0.59\times10^{12}\ M_\odot$. The important point is the perfect coincidence of this mass estimate with the sum of the individual masses of $M_{\rm MW+M31} = (2.34\pm0.41)\times10^{12}\ M_\odot$ obtained completely independently. This indicates that the method works well and gives a result close to the expected mass. Moreover, it follows that essentially the entire mass of the Local Group is concentrated around the two main galaxies.

Table 1. List of galaxies outside virial zones of MW and M 31

Name	J2000.0	$(m-M)_0$	Method		v_h		D_{MW}	D_{M31}
		mag			km s^{-1}		kpc	
WLM	000158.1−152740	24.96 +0.07 −0.07	TRGB	*a*	−122.0 ±2.0	α	981	865
And XVIII	000214.5+450520	25.43 +0.05 −0.03	HB	*b*	−332.1 ±2.7	β	1222	465
Cetus	002611.0−110240	24.48 +0.10 −0.10	TRGB	*a*	−83.9 ±1.2	γ	788	691
IC 1613	010447.8+020800	24.32 +0.05 −0.05	RR Lyr	*c*	−231.0 ±1.0	δ	734	511
Triangulum III	012141.3+262332	24.92 +0.07 −0.07	TRGB	*d*	138.6 ±0.5	ϵ	966	315
Phoenix	015106.3−442641	23.06 +0.12 −0.12	TRGB	*e*	−21.2 ±1.0	ζ	409	859
Perseus I	030123.6+405918	24.24 +0.06 −0.06	RR Lyr	*c*	−325.9 ±3.0	η	711	340
Eridanus II	034421.1−433159	22.80 +0.10 −0.10	BHB	*f*	75.6 ±1.3	θ	365	880
UGC 4879	091602.2+525024	25.68 +0.03 −0.03	TRGB	*a*	−29.2 ±1.6	γ	1373	1398
Leo K	092406.1+163038	23.16 +0.14 −0.55	CMD	*g*			434	986
Leo T	093453.4+170305	23.10 +0.10 −0.10	TRGB	*e*	38.1 ±2.0	ι	422	984
Leo A	095926.4+304447	24.44 +0.11 −0.11	RR Lyr	*h*	23.9 ±0.1	ι	777	1175
Leo M	110521.2+252043	23.30 +0.41 −0.09	CMD	*g*			460	1025
Sag dIG	192959.0−174041	25.17 +0.08 −0.08	TRGB	*e*	−79.0 ±1.0	α	1074	1365
NGC 6822	194457.7−144811	23.58 +0.07 −0.07	TRGB	*a*	−54.5 ±1.7	γ	513	923
DDO 210	204651.8−125053	24.95 +0.14 −0.14	TRGB	*a*	−139.5 ±2.0	κ	972	1099
And XXVIII	223241.2+311258	24.36 +0.05 −0.05	RR Lyr	*c*	−331.1 ±1.8	λ	745	368
Tucana	224149.0−642512	24.82 +0.03 −0.03	TRGB	*a*	194.0 ±4.3	μ	916	1378
Pegasus	232834.1+144448	24.74 +0.05 −0.05	RR Lyr	*c*	−184.5 ±0.3	β	888	458
Pegasus W	235315.0+220607	24.81 +0.14 −0.22	CMD	*i*			918	349

Distance references: *a*) Anand et al. (2021); *b*) Weisz et al. (2019); *c*) Savino et al. (2022); *d*) Collins et al. (2024); *e*) McConnachie & Venn (2020); *f*) Crnojević et al. (2016); *g*) McQuinn et al. (2024); *h*) Bernard et al. (2013); *i*) McQuinn et al. (2023).
Velocity references: α) Koribalski et al. (2004); β) Watkins et al. (2013); γ) Kirby et al. (2014); δ) Haynes et al. (2018); ϵ) Alam et al. (2015); ζ) Kacharov et al. (2017); η) Martin et al. (2014); θ) Pace et al. (2022); ι) McConnachie & Venn (2020); κ) Begum et al. (2006); λ) Tollerud et al. (2013); μ) Fraternali et al. (2009).

A natural extension of the analysis is to find the position of the center of mass of the system that minimizes the observed spread of total mass estimates. Given the previous result that the sum of the individual masses of MW and M 31 estimated from the kinematics of the satellites coincides with the mass of the Local Group estimated from the motion of its outer members, we can be confident that the center of mass of the system is located on the line connecting MW and M 31. Varying the mass ratio and, consequently, the position of the center of mass allows us to significantly reduce the spread of mass estimates of the Local Group by 1.6 times $\sigma_M = 0.36 \times 10^{12}\ M_\odot$. The total mass is $M_{LG} = (2.46 \pm 0.13) \times 10^{12}\ M_\odot$. The result is shown in Fig. 4.

We do not detect any statistically significant trend of the mass with distance from the center of mass of the Local Group. This indicates that over a wide range of distances from 400 kpc to 1.4 Mpc, the total mass of the system is confined within a region of the order of 400 kpc, effectively inside the virial zones around the MW and M 31.

The minimum scatter is reached when the MW-to-M 31 mass ratio is equal to $M_{MW}/M_{M31} = 0.79 \pm 0.10$, which corresponds to the position of the center of mass at the distance of 436 kpc and the velocity of 61 km s^{-1} in the direction of M 31. This allows us to estimate individual masses $M_{MW} = 1.08 \times 10^{12}\ M_\odot$ and $M_{M31} = 1.38 \times 10^{12}\ M_\odot$.

4. Comparison with HESTIA simulations

We compare with ΛCDM simulations of the Local Group, known as the HESTIA simulations (Libeskind et al. 2020). The HESTIA runs are constrained Magneto-Hydro-dynamic simulations of the Local Group performed in a constrained environment which mimics the observed one quite closely. The simulations have been run with the AURIGA (Grand et al. 2017) model of galaxy formation. The initial conditions were created by mapping the $z = 0$ gravitational environment via a Wiener Filter reconstruction from CosmicFlows–2 survey of peculiar velocities (Tully et al. 2013), via a reverse Zeldovich approximation (Doumler et al. 2013).

The simulations result in a local group constituting of two spiral galaxies whose mass (i.e. 0.8–1.2 × $10^{12}\ M_\odot$), mass ratio (∼ 1:1) and separation (∼ 700–800 kpc) are consistent with measured observational properties. Furthermore, properties such as circular velocity, size and star formation history are also all within the observed values. Further afield, the location of a Virgo-like cluster, as well as other cosmographic features (local void, sheet and filament) are all natural outcomes of the constraining technique. Since these are high resolution simulations (achieving a mass resolution of $m_{dm} = 1.2 \times 10^6$ and $m_{gas} = 1.8 \times 10^5\ M_\odot$ for dark matter and gas, respectively) the Local Group (and beyond) is also populated by an entourage of low mass dwarf and satellite galaxies.

In Figure 5, we show an example of the halo velocity-distance diagram in the neighborhood of the Local Group analog obtained in the high-resolution HESTIA simulation 09_18. This plot mimics the real observations when the observer is at the center of the second-mass halo in the group, and the line-of-sight halo velocities and distances are recalculated to the center of mass of the system, similar to Fig. 3. The halos with stars, $M_* \geq 1.5 \times 10^5$, are shown by color circles only outside the virial zones of 300 kpc around of two most massive halos. The large circles show halos at $D \geq 450$ kpc from the central halos. They correspond to the real galaxies used to estimate the Local Group mass. The small colored circles represent 'satellites' in the vicinity of the two central galaxies, $300 \leq D \leq 450$ kpc. The virial zones of the two massive halos overlap and are centered at a distance of about 400 kpc relative to the center of mass. Just outside the virial zones, one can see a well pronounced flow of objects as they fall into the group. Above this flow there are a number of outliers representing, among others, the backsplash objects. Star-forming halos track the general behavior of all halos well. It can

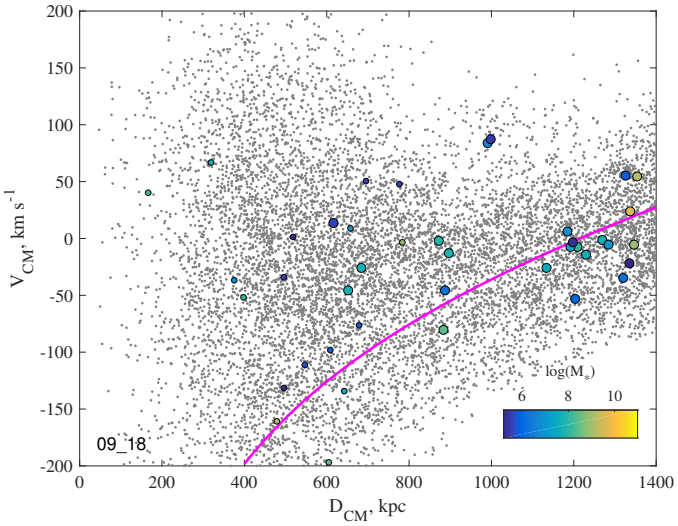

Fig. 5. The Hubble flow in the neighborhood of the Local Group analog in the high-resolution HESTIA simulations 09_18. Colored circles indicate halos with stellar particles, $M_* \geq 1.5\times10^5\ M_\odot$, but only outside the virial zones of 300 kpc around of two most massive halos. The large circles correspond to distant members $D \geq 450$ kpc away from the MW and M 31 analogs, while the small circles indicate closer objects.

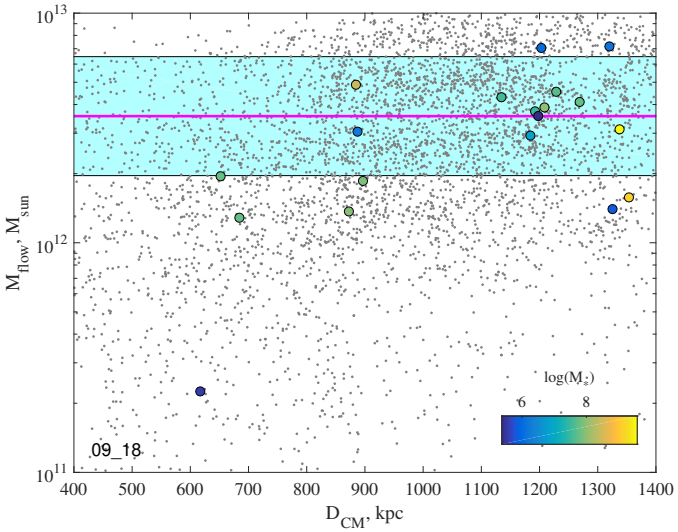

Fig. 6. Estimation of the mass of the system from the Hubble flow, as in Fig. 4, but using the HESTIA simulation data.

be seen that the simulations reproduce the observed velocity-distance diagram quite well. The main difference between the simulations and the Local Group is in the significantly larger velocity spread of the infalling galaxies. The typical value in the simulations is about 70 versus 14 km s^{-1} for galaxies outside the virial zones in the Local Group.

5. Discussion

First of all, it is necessary to draw attention to the existence of two populations of galaxies outside the virial zones of the Milky Way and the Andromeda Galaxy. Two-thirds of known galaxies follow a regular Hubble flow relative to the barycenter of the Local Group. The spread of line-of-sight velocities is only 14 km s^{-1} and may partially be due to errors in the distances to the objects.

Table 2. Comparison of mass estimations using the Hubble flow model with the HESTIA simulations

Set	M_1+M_2	$M(r<1)$		$\langle M_{\rm flow}\rangle$	σ
	$\times10^{12}\ M_\odot$			$\times10^{12}\ M_\odot$	
09_18	2.76	3.33	4980	3.27 ± 0.04	2.62
	$M_* \geq 1.5\times10^5$		21	3.51 ± 0.41	1.95
17_11	2.89	3.33	4902	3.54 ± 0.04	3.42
	$M_* \geq 1.5\times10^5$		15	4.87 ± 1.00	4.37
37_11	1.40	2.08	4028	2.72 ± 0.03	2.18
	$M_* \geq 1.5\times10^5$		27	2.36 ± 0.29	1.68

The extremely cold Hubble flow in the nearby Universe was pointed out by Karachentsev & Makarov (2001); Karachentsev et al. (2002), who discovered a line-of-sight dispersion of 25–30 km/s in the expansion of isolated nearby galaxies up to ∼3 Mpc, based on precise the Tip of the Red Giant Branch (TRGB) distances. Ekholm et al. (2001) found the velocity dispersion of 38 km s^{-1} in the distance range 1–8 Mpc using Cepheid distances. Such a regular and cold Hubble expansion in the face of the highly non-uniform environment in the nearby Universe seemed mysterious. Attention to this problem goes back as far as Sandage et al. (1972). Baryshev et al. (2001) suggested that this enigma is explained by adiabatic cooling of the chaotic motions of galaxies in regions dominated by dark energy. In contrast, the insignificant contribution of Λ to the formation of the density profile and velocity field around galaxy clusters was pointed out as early as Lahav et al. (1991). Using constrained cosmological simulations, Hoffman et al. (2008) showed that dark energy does not manifest itself in any way in the dynamics of the local Universe, and the dispersion of $\lesssim$ 60 km s^{-1} in the range from 0.75 to 2 or 3 Mpc is found in more than half of the cases. Thus, they conclude that the problem of the cold Hubble flow is not related to dark energy, but rather to the mean matter density around objects.

It is important to emphasize here that we observe the cold Hubble flow with a dispersion of only 14 km s^{-1} inside the zero-velocity sphere of the Local Group at distances from 400 to 1400 kpc. If this is not a statistical anomaly, such small chaotic velocities seem surprising, even considering that the Local Group is 3–4 Mpc away from its nearest massive neighbors. Current cosmological models demonstrate the flow of matter into groups and clusters of galaxies. But, even in constrained simulations, such as HESTIA, which imitate the Local Group environment well, this inflow does not appear to be as cold.

Despite the above, not all galaxies follow the Hubble flow. The positions and velocities of the four galaxies cannot be described by the model under any reasonable parameters. Apparently, this may indicate that they are not at the stage of the first infall into the Local Group and have experienced interactions with its members before.

Tucana is an isolated dSph galaxy on the border of the Local Group. Makarova & Makarov (2021) found that it does not show any sign of residual star formation in the last 2 Gyr, which differs it significantly from other isolated dSph galaxies, KKR 25, KK 258, and KKs 3, as well as And XVIII, which is located within the Local Group but well outside the virial zone of M 31. Tucana's star formation is typical of dSph satellites of giant galaxies that have lost their gas due to ram pressure stripping and tidal interaction with a massive galaxy. Note that And XVIII follows the Hubble flow perfectly.

Cetus, like Tucana, is an isolated dSph galaxy located within the Local Group. It does not follow the Local Group morphology-density relation. Taibi et al. (2018) note tidal tail-

like structures in the outer part of the galaxy, although their presence is difficult to reconcile with the timescales of a possible passage around M 31, and the orbit of Cetus through the Local Group indicates that it is at the apocentre (Lewis et al. 2007). Gallart et al. (2015) suggested that the line-of-sight velocities of Tucana and Cetus are compatible with the assumption that they were close to the barycenter of the Local Group at early times, probably when they just assembled. Likewise, Teyssier et al. (2012) suggested that Tucana, Cetus, NGC 6822 are possibly backsplash galaxies, based on their current observed positions and radial velocities. Data, presented in the study of Komiyama et al. (2003), support the scenario that a passage of the northwest H I cloud produced the 'tidal arm' to the southeast of NCG 6822 and triggered the recent star formation activity found in the entire galaxy. At the same time, McConnachie et al. (2021) find that NGC 6822 is highly likely to be isolated and on its first infall, based on orbital properties derived using Gaia Data Release 2 proper motions of the brightest stars.

Kniazev et al. (2009) studied the stellar component of the very faint outer regions of the Pegasus dwarf (Peg DIG), as well as its H I component. The authors rule out a possible tidal origin or a ram pressure stripping scenario, and propose that the Pegasus dwarf is on its first infall in the Local group since it does not appear to be disturbed by interactions with other galaxies. However, it is also worth to note that, according to the studies mentioned above, NGC 6822 and Peg DIG are dark-matter dominated objects.

Thus, the four outliers, Cetus, Tucana, Peg DIG and NGC 6822 are distinct from other studied external galaxies, and the reasons may be suspected in their evolution in the Local Group (backsplash galaxies) as well as in their assembly and star formation details (dark matter-dominated objects).

The arguments presented above give us reason to believe that we obtain a reliable estimate of the total mass of the Local Group $M_{\rm LG} = (2.46 \pm 0.13) \times 10^{12}\ M_\odot$ by studying the kinematics of the peripheral members of the Local Group.

The idea of using deviations from the ideal linear Hubble flow to estimate the total mass of the Local Group dates back to Lynden-Bell (1981) and Sandage (1986). The radius of the zero-velocity sphere, determined from the recession of nearby galaxies, has been used many times for this purpose. Karachentsev et al. (2009) measured it as $R_0 = (0.96 \pm 0.03)$ Mpc, which gave a total mass of $M_{\rm LG} = (1.9 \pm 0.2) \times 10^{12}\ M_\odot$. Kashibadze & Karachentsev (2018) obtained even smaller values of $R_0 = (0.91 \pm 0.05)$ Mpc and $M_{\rm LG} = (1.5 \pm 0.2) \times 10^{12}\ M_\odot$, and noted the paradoxical situation when the total mass turns out to be less than the sum of the virial masses of MW and M 31. In our work, we take into account the influence of dark energy more carefully and use the analytical model of the Hubble flow (Baushev 2020), which give us a larger and more precise estimate of the total mass of the Local Group, which, in turn, eliminated the above-mentioned paradox (see below). Benisty et al. (2024) refine the definition of zero-acceleration and zero-velocity surfaces for a general mass distribution on a cosmological background governed by a cosmological constant. They estimated the total mass of the Local Group to be $M_{\rm LG} = (2.47 \pm 0.08) \times 10^{12}\ M_\odot$, which matches our value perfectly.

Another classic approach to weighing the Local Group is the so-called timing argument, proposed by Kahn & Woltjer (1959). It is based on the assumption that the observed configuration of the Milky Way and the Andromeda Galaxy is the result of their first encounter while moving along radial Keplerian orbits during the lifetime of the Universe. This method usually produces a significantly larger mass of the Local Group of about $5 \times 10^{12}\ M_\odot$ compared to other methods (Sawala et al. 2023). So, Benisty et al. (2022) estimate the total mass of $(3.7 \pm 0.5) \times 10^{12}\ M_\odot$ taking into account the proper motion of M 31 provided by the Gaia mission. However, careful consideration of the influence of the Large Magellanic Cloud reduces this value to $(2.3 \pm 0.7) \times 10^{12}\ M_\odot$ (Benisty 2024), making the timing argument comparable with other estimates and, in turn, agreeing within error with our value.

We would like to emphasize two important results of our work: 1) the absence of a significant trend in the estimate of the total mass of the Local Group in the distance range from 400 to 1400 kpc; 2) the equality of the Local Group mass of $M_{\rm LG} = (2.46 \pm 0.13) \times 10^{12}\ M_\odot$ estimated from the Hubble flow to the sum of the individual masses of the Milky Way and the Andromeda Galaxy, $M_{\rm MW+M31} = (2.34 \pm 0.41) \times 10^{12}\ M_\odot$ (Makarov et al. 2025), measured from the kinematics of their satellites. This indicates that almost all of the mass of the Local Group is concentrated within the virial zones of its two main galaxies. Karachentsev (2005); Karachentsev et al. (2009) previously drew attention to the equality of virial masses of galaxy groups on scales of 200–300 kpc as well as total masses inside a zero-velocity sphere with a radius of about 1 Mpc. This is probably also true for larger structures such as the Virgo cluster (Karachentsev & Nasonova 2010).

The fact that all the mass is concentrated around MW and M 31 allows us to determine their mass ratio of $M_{\rm MW}/M_{\rm M31} = 0.79 \pm 0.10$ by finding the barycenter of the Local Group to minimize the spread of the mass estimates from the Hubble flow model. It corresponds to the individual masses of $M_{\rm MW} = (1.08 \pm 0.15) \times 10^{12}\ M_\odot$ and $M_{\rm M31} = (1.38 \pm 0.11) \times 10^{12}\ M_\odot$ for the Milky Way and the Andromeda Galaxy, respectively. This MW mass is somewhat greater than the mass estimated from the kinematics of its satellites excluding Leo I, $(0.79 \pm 0.23) \times 10^{12}\ M_\odot$ (Makarov et al. 2025), although it remains in agreement. However, if Leo I is included in the consideration, the MW mass increases to $(1.07 \pm 0.30) \times 10^{12}\ M_\odot$, which perfectly matches the estimate from the barycenter position. This is also consistent with numerous measurements of the MW mass within 200 kpc made by other authors and collected in recent reviews. The compilation by Wang et al. (2020) gives an average of $\langle M_{\rm MW} \rangle = 1.07 \times 10^{12}\ M_\odot$ with a spread of $\sigma_{\rm MW} = 0.30 \times 10^{12}\ M_\odot$, and Bobylev & Baykova (2023) point out a mean of $\langle M_{\rm MW} \rangle = 0.88 \times 10^{12}\ M_\odot$ with a dispersion of $\sigma_{\rm MW} = 0.24 \times 10^{12}\ M_\odot$. The M 31 mass estimated from the barycenter position also agrees well with the kinematics of its satellites within 300 kpc, both from the literature, $\langle M_{\rm M31} \rangle = 1.61 \times 10^{12}\ M_\odot$, $\sigma_{\rm M31} = 0.24 \times 10^{12}\ M_\odot$ (see review by Bhattacharya 2023), and from our measurements $M_{\rm M31} = (1.55 \pm 0.34) \times 10^{12}\ M_\odot$ (Makarov et al. 2025).

The barycenter of the Local Group determined from seven dwarfs is located at 436 ± 27 kpc between MW and M 31, where the adopted distance to M 31 is 776 ± 22 kpc (Savino et al. 2022). $D_{\rm BC} = (0.56 \pm 0.03) D_{\rm M31}$ is in excellent agreement with Karachentsev et al. (2009), who determined it to be equal to 0.55 ± 0.05 using 30 neighboring galaxies with distances in range 0.7–3.0 Mpc. Taking into account that the approach velocity of MW and M 31 is -109 ± 2 km s^{-1}, we find that the Milky Way is moving at a speed of 61.1 ± 2.5 km/s towards the barycenter of the Local Group $(l, b) = (+121.7^\circ \pm 2.1^\circ, -21.5^\circ \pm 1.4^\circ)$. Combining this with the motion of the Sun in the Galaxy, we obtain the solar vector relative to the barycenter of the Local Group equal to $(V_x, V_y, V_z) = (-20.4 \pm 3.5, +299.1 \pm 3.2, -13.8 \pm 1.3)$ in the Galactic coordinates, which in the sky corresponds to

$(l, b, V) = (+93.9^\circ \pm 0.7^\circ, -2.6^\circ \pm 0.3^\circ, 300 \pm 3\ \mathrm{km\,s^{-1}})$. This is in excellent agreement with the apex of the Sun relative to the centroid of the Local Group, $(+93^\circ \pm 2^\circ, -4^\circ \pm 2^\circ, 316 \pm 5\ \mathrm{km\,s^{-1}})$, found by Karachentsev & Makarov (1996).

6. Conclusions

We analyze the motions of 11 peripheral members of the Local Group at distances from 400 to 1400 kpc from its center. The positions and velocities of 7 of them are perfectly described by an analytical model of the Hubble flow around a spherical overdensity in the standard flat ΛCDM universe (Baushev 2020). The remaining 4 galaxies have most likely been influenced earlier by other members of the Local Group and cannot be considered as free-falling particles. In the following, we summarize our conclusions.

- Despite the dumbbell-shaped structure of the Local Group, the spherically symmetric Hubble flow model (Baushev 2020) relative to the barycenter of the Local Group gives a very good description of the velocity field inside its zero-velocity sphere down to the boundaries of the virial zones around the Milky Way and the Andromeda Galaxy.
- The Hubble flow in the vicinity of the Local Group from 400 to 1400 kpc is extremely cold with a line-of-sight velocity dispersion of only 14 $\mathrm{km\,s^{-1}}$. This is actually an upper limit, as distance errors should contribute significantly.
- Constrained cosmological ΛCDM simulations predict a much larger scatter of the velocity field, on the order of 70 $\mathrm{km\,s^{-1}}$, outside the virial radii of the MW and M 31.
- Most mass estimates derived from the velocity and position of individual galaxies relative to the Local Group barycenter agree well with each other with extremely small scatter of $\sigma_M = 0.36 \times 10^{12}\ M_\odot$. This allows us to estimate the total mass of the Local Group as $M_{\mathrm{LG}} = (2.46 \pm 0.13) \times 10^{12}\ M_\odot$.
- There is no statistically significant change in the mass of the Local Group in the distance range from 400 to 1400 kpc.
- The Hubble flow model is in remarkable agreement with the sum of the total masses of our Galaxy and the Andromeda Galaxy, estimated from the kinematics of their satellites. From this we conclude that almost the entire mass of the Local Group is concentrated within 400 kpc around these two giant spirals, in fact within their virial radii.
- The barycenter of the Local Group, determined from the condition of minimizing the spread of mass estimates, corresponds to the mass ratio between the Milky Way and the Andromeda Galaxy equal to $M_{\mathrm{MW}}/M_{\mathrm{M31}} = 0.79 \pm 0.10$. Our Galaxy is moving towards the barycenter at a speed of $61.1 \pm 2.5\ \mathrm{km\,s^{-1}}$. Thus, the solar apex relative to the barycenter of the Local Group is equal to $(l, b, V) = (+93.9^\circ \pm 0.7^\circ, -2.6^\circ \pm 0.3^\circ, 300 \pm 3\ \mathrm{km\,s^{-1}})$ in the Galactic coordinates.

Acknowledgements. This work was supported by the Russian Science Foundation grant № 24–12–00277.

References

Akhmetov, V. S., Bucciarelli, B., Crosta, M., et al. 2024, MNRAS, 530, 710
Alam, S., Albareti, F. D., Allende Prieto, C., et al. 2015, ApJS, 219, 12
Anand, G. S., Rizzi, L., Tully, R. B., et al. 2021, AJ, 162, 80
Bahcall, J. N. & Tremaine, S. 1981, ApJ, 244, 805
Baryshev, Y. V., Chernin, A. D., & Teerikorpi, P. 2001, A&A, 378, 729
Battaglia, G., Taibi, S., Thomas, G. F., & Fritz, T. K. 2022, A&A, 657, A54
Baushev, A. N. 2020, Phys. Rev. D, 102, 083529
Begum, A., Chengalur, J. N., Karachentsev, I. D., Kaisin, S. S., & Sharina, M. E. 2006, MNRAS, 365, 1220
Benisty, D. 2024, A&A, 689, L1
Benisty, D., Chaichian, M. M., & Tureanu, A. 2024, Physics Letters B, 858, 139033
Benisty, D., Vasiliev, E., Evans, N. W., et al. 2022, ApJ, 928, L5
Bernard, E. J., Monelli, M., Gallart, C., et al. 2013, MNRAS, 432, 3047
Bhattacharya, S. 2023, arXiv e-prints, arXiv:2305.03293
Bobylev, V. V. & Baykova, A. T. 2023, Astronomy Reports, 67, 812
Collins, M. L. M., Karim, N., Martinez-Delgado, D., et al. 2024, MNRAS, 528, 2614
Crnojević, D., Sand, D. J., Zaritsky, D., et al. 2016, ApJ, 824, L14
Doumler, T., Hoffman, Y., Courtois, H., & Gottlöber, S. 2013, MNRAS, 430, 888
Ekholm, T., Baryshev, Y., Teerikorpi, P., Hanski, M. O., & Paturel, G. 2001, A&A, 368, L17
Fraternali, F., Tolstoy, E., Irwin, M. J., & Cole, A. A. 2009, A&A, 499, 121
Gaia Collaboration, Brown, A. G. A., Vallenari, A., et al. 2018, A&A, 616, A1
Gallart, C., Monelli, M., Mayer, L., et al. 2015, ApJ, 811, L18
Grand, R. J. J., Gómez, F. A., Marinacci, F., et al. 2017, MNRAS, 467, 179
GRAVITY Collaboration, Abuter, R., Amorim, A., et al. 2021, A&A, 647, A59
Haynes, M. P., Giovanelli, R., Kent, B. R., et al. 2018, ApJ, 861, 49
Hoffman, Y., Martinez-Vaquero, L. A., Yepes, G., & Gottlöber, S. 2008, MNRAS, 386, 390
Kacharov, N., Battaglia, G., Rejkuba, M., et al. 2017, MNRAS, 466, 2006
Kahn, F. D. & Woltjer, L. 1959, ApJ, 130, 705
Karachentsev, I. & Makarov, D. 2001, Astrofizika, 44, 1
Karachentsev, I. D. 2005, AJ, 129, 178
Karachentsev, I. D., Kashibadze, O. G., Makarov, D. I., & Tully, R. B. 2009, MNRAS, 393, 1265
Karachentsev, I. D. & Makarov, D. A. 1996, AJ, 111, 794
Karachentsev, I. D. & Nasonova, O. G. 2010, MNRAS, 405, 1075
Karachentsev, I. D., Sharina, M. E., Makarov, D. I., et al. 2002, A&A, 389, 812
Kashibadze, O. G. & Karachentsev, I. D. 2018, A&A, 609, A11
Kirby, E. N., Bullock, J. S., Boylan-Kolchin, M., Kaplinghat, M., & Cohen, J. G. 2014, MNRAS, 439, 1015
Kniazev, A. Y., Brosch, N., Hoffman, G. L., et al. 2009, MNRAS, 400, 2054
Komiyama, Y., Okamura, S., Yagi, M., et al. 2003, ApJ, 590, L17
Koribalski, B. S., Staveley-Smith, L., Kilborn, V. A., et al. 2004, AJ, 128, 16
Lahav, O. & Liddle, A. R. 2022, arXiv e-prints, arXiv:2201.08666
Lahav, O., Lilje, P. B., Primack, J. R., & Rees, M. J. 1991, MNRAS, 251, 128
Lewis, G. F., Ibata, R. A., Chapman, S. C., et al. 2007, MNRAS, 375, 1364
Libeskind, N. I., Carlesi, E., Grand, R. J. J., et al. 2020, MNRAS, 498, 2968
Lynden-Bell, D. 1981, The Observatory, 101, 111
Makarov, D., Makarov, D., Kozyrev, K., & Libeskind, N. 2025, arXiv e-prints, arXiv:2503.12612
Makarova, L. N. & Makarov, D. I. 2021, MNRAS, 502, 1623
Martin, N. F., Chambers, K. C., Collins, M. L. M., et al. 2014, ApJ, 793, L14
McConnachie, A. W., Higgs, C. R., Thomas, G. F., et al. 2021, MNRAS, 501, 2363
McConnachie, A. W. & Venn, K. A. 2020, AJ, 160, 124
McQuinn, K. B. W., Mao, Y.-Y., Buckley, M. R., et al. 2023, ApJ, 944, 14
McQuinn, K. B. W., Mao, Y.-Y., Tollerud, E. J., et al. 2024, ApJ, 967, 161
Pace, A. B., Erkal, D., & Li, T. S. 2022, ApJ, 940, 136
Reid, M. J. & Brunthaler, A. 2020, ApJ, 892, 39
Salomon, J. B., Ibata, R., Reylé, C., et al. 2021, MNRAS, 507, 2592
Sandage, A. 1986, ApJ, 307, 1
Sandage, A., Tammann, G. A., & Hardy, E. 1972, ApJ, 172, 253
Savino, A., Weisz, D. R., Skillman, E. D., et al. 2022, ApJ, 938, 101
Sawala, T., Teeriaho, M., & Johansson, P. H. 2023, MNRAS, 521, 4863
Taibi, S., Battaglia, G., Kacharov, N., et al. 2018, A&A, 618, A122
Teyssier, M., Johnston, K. V., & Kuhlen, M. 2012, MNRAS, 426, 1808
Tollerud, E. J., Geha, M. C., Vargas, L. C., & Bullock, J. S. 2013, ApJ, 768, 50
Tully, R. B., Courtois, H., Hoffman, Y., & Pomarède, D. 2014, Nature, 513, 71
Tully, R. B., Courtois, H. M., Dolphin, A. E., et al. 2013, AJ, 146, 86
Wang, W., Han, J., Cautun, M., Li, Z., & Ishigaki, M. N. 2020, Science China Physics, Mechanics, and Astronomy, 63, 109801
Watkins, L. L., Evans, N. W., & van de Ven, G. 2013, MNRAS, 430, 971
Weisz, D. R., Dolphin, A. E., Martin, N. F., et al. 2019, MNRAS, 489, 763